The Journal of Physical Chemistry A

 VOLUME 103, NUMBER 22, JUNE 3, 1999

FEATURE ARTICLE

Triphenylmethane Dyes Revealing Heterogeneity of Their Nanoenvironment: Femtosecond, Picosecond, and Single-Molecule Studies

Mitsuru Ishikawa,*,† Jing Yong Ye,† Yoshihiro Maruyama,‡ and Hiroki Nakatsuka§

Joint Research Center for Atom Technology (JRCAT)-Angstrom Technology Partnership (ATP), 1-1-4 Higashi, Tsukuba, Ibaraki 305-0046, Japan, Hamamatsu Photonics K. K., Tsukuba Research Laboratory, 5-9-2 Tokodai, Tsukuba, Ibaraki 300-2635, Japan, and Institute of Applied Physics, University of Tsukuba, 1-1-1 Ten-nodai Tsukuba, Ibaraki 305-0006, Japan

Received: December 7, 1998; In Final Form: March 19, 1999

This article describes several lines of our recent work on pico- and femtosecond spectroscopy of triphenylmethane dyes. Furthermore, we reduced the number of molecules in the ensemble-averaged studies to the single-molecule regime. The single-molecule technique would allow us to reveal intrinsic characteristics of individual chromophores embedded in glass, polymers, and liquid.

General Introduction

Flexibility of molecular frameworks including functional groups is one of particular characteristics of organic molecules in contrast to metals and semiconductors. Among many classes of organic molecules, we exclusively consider the molecules whose size is larger than the size of benzene because flexibility may become important for the molecules larger than benzene. Furthermore, standard ultraviolet−visible spectroscopies are applicable to studying this class of molecules. The intrinsic flexibility of molecular structures and the availability of the standard ultraviolet−visible spectroscopies make it possible to use such molecules as exquisitely sensitive probes of the immediate local environments around them, particularly when they are prepared in the single-molecule regime. In this article we highlight triphenylmethane (TPM) dyes, the structure of which is characterized by three-blade propeller-like phenyl rings joined by a central carbon atom (Figure 1). The photochemistry and photophysics of TPM dyes in solid and liquid media were described in a recent review article.[1] Flexibility of TPM dyes comes from this peculiar structure. Some physical chemists who engaged in time-resolved spectroscopy have long been interested in the relaxation mechanisms of the excited states of TPM dyes. Indeed, TPM dyes were studied again and again whenever ultrashort-pulse lasers were newly developed from the picosecond[2] to femtosecond era,[3] because the relaxation times of TPM dyes are conveniently adjustable to fit the available pulse width of the lasers used simply by changing the solvent viscosity. The fluorescence lifetime (τ_f) of TPM dyes depends strongly on the solvent viscosity from several picoseconds in methanol (0.6 cP)[4−7] at 293 K to ∼4.0 ns in alcohols and polymers below 100 K.[8−11] The extreme sensitivity of τ_f to viscosity is the very reason for the applicability of TPM dyes as molecular probes for viscosity in condensed matter such as liquid, polymers, and glass. Also, oscillating wavelengths of available ultrashort-pulse lasers were suitably fitted with the absorption maximums of TPM dyes (Figure 2). Recently, we have implemented imaging and spectroscopy of single dye molecules on the basis of fluorescence measurement[12−15] and found a single TPM dye molecule to be useful as a probe for the local viscosity of polymer matrixes in which it is embedded.[14] In this article we follow our route to the single-molecule

* Corresponding author. E-mail: ishikawa@jrcat.or.jp.
† JRCAT-ATP.
‡ Hamamatsu Photonics K. K., Tsukuba Research Laboratory.
§ University of Tsukuba.

10.1021/jp984650p CCC: $18.00
Published on Web 05/15/1999

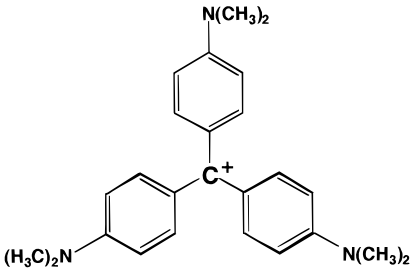

Crystal Violet (CV)

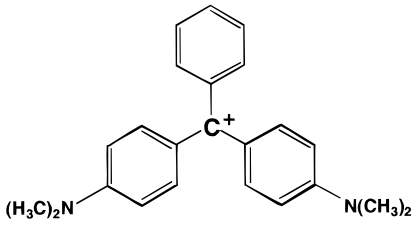

Malachite Green (MG)

Figure 1. Molecular structures of selected TPM dyes.

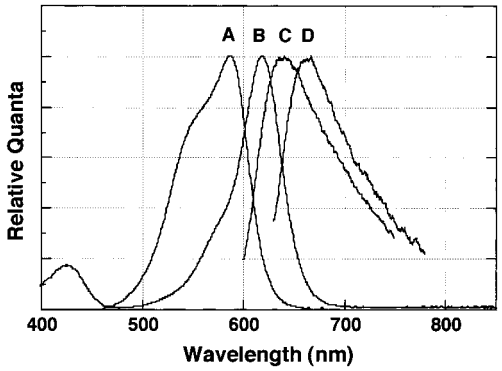

Figure 2. Absorption spectrum of CV (A) and of MG (B) in methanol at 295 K. Fluorescence spectrum of CV (C) and of MG (D) in glycerol at 295 K.

study starting from pico- and femtosecond spectroscopies as motives for the single-molecule study.

The main body of this article is composed of three parts. First, we present how the molecular structure of crystal violet (CV), which is one of the TPM dyes selected, is sensitive to its surrounding solvent molecules in solution. Recently, a subtle structural difference in the ground state of CV was identified in alcohols by means of a femtosecond spectral hole-burning technique.[16,17] Two-fold key points of these studies are (i) proposal for a novel class of isomers that are differentiated one from the other by solvation and (ii) conclusive decision of a long-run dispute whether the ground-state conformational isomers exist. Second, another TPM dye, malachite green (MG), was used as a molecular probe for the glass transition of alcohols and polymers.[10,11] Analysis of the temperature dependence of nonradiative relaxation in MG shed light on the mechanism of glass transition. Novel experimental observations are grouped into two classes. (i) The critical temperature (T_c) predicted by the mode-coupling theory (MCT) was undoubtedly observed 30−50 K above the calorimetric glass transition temperature (T_g) for monomer alcohols and a polymer without side chains. On this occasion fluorescence decay curves were expressed with a biexponential function above T_g, whereas with a single exponential below T_g. (ii) In polymers with side chains, however, T_c is not found above T_g but another transition temperature was observed below T_g in contrast to the monomers and the polymer without side chains. In such a case, fluorescence decay curves were expressed with a biexponential function above and below T_g. Last, we extended the second study to the single-molecule regime using CV as a single-molecule probe.[14] On the basis of the biexponential fluorescence decay curves above and below T_g we assume that polymers with side chains have two sites: one is a liquidlike site, which causes fast fluorescence decays, and the other is a solidlike site, which causes slow fluorescence decays. We succeeded in identifying the above assumption at room temperature (23 °C) by examining fluorescence properties of individual CV molecules embedded in poly(methyl methacrylate) (PMMA), for which $T_g = 114$ °C.[18]

Experimental Setups

In the section Solvation Isomers of a TPM Dye in Alcohols, we used several alcoholic (methanol, ethanol, *n*-propanol, and *n*-butanol) solutions of CV as samples. The sample concentration was 5×10^{-4} M. No spectral change was observed in absorption for alcohol solutions of CV over the concentration range from 10^{-3} to 10^{-5} M. This shows no aggregation of CV in the alcohols used. The samples were circulated through a 0.5-mm thick quartz cell to avoid persistent photobleaching. The femtosecond dye laser system and femtosecond pump−probe spectrometer that we employed were described elsewhere.[16,17]

We also studied the effects of a solvent molecule on the molecular structure of CV by molecular orbital calculations. The solvent molecule was methanol. The calculation method used was MNDO-PM3 (modified neglect of diatomic overlap, parametric method 3)[19] with the program MOPAC Version 6. Optical transition energies of CV were calculated using CNDO/S-CI (complete neglect of differential overlap/spectroscopic-included configuration interaction).[20] The one hundred lowest energies of one-electron-excited configuration were taken into account for the configuration interaction calculations. A new g value ($g = e^2/(R_{rs} + ka_{rs})$) was used for two-centered electron repulsion integral.[21] The k value that reproduced the experimental absorption maximums was 2.75. Even when $k = 1$ and the ordinary Nishimoto−Mataga g value[21] were used, final results were essentially not affected, except for the absolute energies of absorption maximums. Following ref 22 MNDO-PM3 is reliable in the calculations of molecular structures in the ground state, but not so in the calculations including hydrogen bonding, transition structures, molecules containing atoms that are poorly parametrized. Also the use of CNDO/S-CI is adequate for the calculations of optical transition energies and oscillator strength, even when the molecules involved are nonplanar like ours because both π and σ electrons are considered in this method.[20,21] Alternatively, the use of PPP-CI (Pariser−Parr−Pople configuration interaction) method[23,24] is possible, but PPP-CI is not sufficient for nonplanar molecules because this method considers only π electrons.

In the section Probing Glass Transition in Alcohols and Polymers Using a TPM Dye, we used a mode-locked dye laser (Coherent, Satori) synchronously pumped with a continuous-wave (cw) mode-locked and frequency-doubled Nd:YAG laser (Coherent, Antares) at a repetition rate of 76 MHz. The output pulses of the dye laser (250-fs fwhm and 642 nm) were attenuated to a few milliwatts and focused on the sample in a cryostat. The fluorescence photons emitted were dispersed with a polychromator (Chromex, 250IS) and time-resolved with a synchroscan streak camera (Hamamatsu, C1587). When measuring slow fluorescence decays at lower temperatures than 273

K, we employed a cw cavity-dumped dye laser (Spectra-Physics, 375B and 344S) that was synchronously pumped with a cw mode-locked argon ion laser (Spectra-Physics, 2030-18). The pulse dye laser, oscillating at 540 nm, was operated at a 4-MHz repetition rate with 10-ps fwhm. The output of the polychromator was time-resolved with a photon-counting streak scope (Hamamatsu, C4334).[13]

In the section Single Molecules Probing Domain Structures in a Polymer Film, we used a pulse-laser system for the fluorescence lifetime measurement. The system was composed of a mode-locked Ti:sapphire oscillator (Coherent, Mira 900F) pumped with a cw argon ion laser (Coherent, Innova 425), a regenerative amplifier (Coherent, RegA 9000) that yields pulses at a 200-kHz repetition rate with 250-fs fwhm, and an optical parametric amplifier (Coherent, OPA 9400) that produces tunable pulses. The output pulses tuned to 540 nm were circularly polarized with a Babinet-Soleil compensator to irradiate uniformly CV molecules. For single-molecule time-resolved fluorometry, the fluorescence photons passing through a pinhole placed in the image plane of an optical microscope (Zeiss Axioplan) was focused on the entrance slit of the polychromator. The polychromator was coupled with the photon-counting streak scope to determine simultaneously the fluorescence spectrum and lifetime of single CV molecules.

For single-molecule imaging experiments, a frequency-doubled (532 nm) diode-laser pumped cw Nd:YAG laser (Coherent, DPSS 532) was used for excitation of samples with the power density of $\sim$6.2 W/cm^2. The laser light was circularly polarized to irradiate equally CV molecules. The emitted fluorescence was determined with an epifluorescence microscope (Nikon, Optiphot XP), equipped with a Nikon BA 580 long-pass filter and a Nikon CF M Plan SLWD 100$\times$ objective with a numerical aperture of 0.75. The microscope was coupled with a photon-counting video camera system (Hamamatsu, C2400-40).

A drop of a methanol solution of CV was spin coated on an $\sim$30-nm-thick PMMA film previously spin coated on a quartz substrate. The dye concentration was 1 mM for fluorescence lifetime measurements in bulk, and 1.0 and 0.1 nM for single-molecule measurements. The use of nanomolar or lower concentrations of solutions is common for preparing well-separated single molecules on substrate surfaces.[25−27]

Solvation Isomers of a TPM Dye in Alcohols

Introduction to a Detective Story Searching for Ground-State Isomers of CV. For CV there have been extensive studies concerning molecular structures,[28−31] electronic states,[32−36] and relaxation dynamics of electronic excited states.[2−11,16,17,37−47] The visible absorption spectrum of CV in solution appears to be composed of two bands, as shown in Figure 2, and the origin of the two bands was interpreted in three different ways: (i) resolution of vibronic structures in one electronic state,[31] (ii) electronic transition from one ground state to two excited states,[32−36] and (iii) the existence of two ground-state isomers.[4,48−50] There is an over 50-year long dispute among (i), (ii), and (iii) as an origin of the 2-fold absorption spectrum.

Lewis and co-workers[48] proposed in 1942, as the beginning of the dispute, two ground-state conformational isomers in thermal equilibrium as an origin of the doubly split absorption bands. One was a propeller structure (D_3 symmetry), in which three phenyl rings are tilted in the same direction. The other was a distorted propeller structure (C_2 symmetry) for which one of the phenyl rings is tilted in the opposite direction. This model was based on the observation that the shorter-wavelength band was diminished and the longer-wavelength band was enhanced with decreasing temperature from 296 to 80 K in alcoholic solutions. This observation argues against the possibility (i) of a resolved vibronic structure as an assignment of the shorter wavelength band. Furthermore, similar intensity exchange between the two bands under high pressure[49,50] was rationally explained within the framework of this model if we consider the modification of chemical equilibrium between two ground-state isomers.

However, several theoretical studies concluded that the two bands originate from electronic transitions from one ground state to two excited states.[29,32−36] The D_3-symmetry conformation was confirmed by an X-ray diffraction study of crystal samples,[28] resonance Raman studies,[30,31,36] and magnetic circular dichroism measurements.[29] On the other hand, the C_2-symmetry conformation has not been identified yet. Leuck and co-workers[36] recently calculated both the energy difference and the potential barrier between the D_3-symmetry conformation and the C_2-symmetry conformation; the latter structure was larger in energy ($\sim$5000 cm^{-1}) than the thermal energy ($\sim$200 cm^{-1}) at room temperature. Thus, the population of the C_2-symmetry conformation, even if possible, would be negligible at room temperature (296 K).

The studies of relaxation dynamics of CV in solution were done by the pico- and femtosecond pump−probe technique.[2−7,37−47] The authors observed that the bleaching recovery probed on the red side of the bleaching spectrum is faster than that probed on the blue side. This observation was explained as being due to either of the two ground states[4] or to two excited states having different nonradiative decay rates.[41] However, Ben-Amotz and Harris[6] explained that the apparent faster relaxation at the red side of the bleaching spectrum would be due to stimulated emission gains concomitant with the bleaching. Besides that observation, there was no excitation and observation-wavelength dependence of the bleaching recovery kinetics. From this observation, the authors concluded that only one ground state and one excited state are enough to explain the observed bleaching recovery dynamics.

Many studies concluded that the D_3-symmetry species only exists and denied the C_2-symmetry structure. They failed, however, to explain the temperature and the pressure dependence of the absorption spectrum, both of which are the substantial evidence for the existence of two ground states. On the other hand, only the temperature and the pressure dependence of the absorption spectrum evidenced the idea of the two ground states. Thus, there has been no model to explain comprehensively all of the previous experimental observations and theoretical calculations. We employed the femtosecond spectral hole-burning technique to confirm whether the absorption spectrum is homogeneous or inhomogeneous. As described above, the relaxation dynamics of CV in the pico- and femtosecond regime was studied. However, no study paid attention to the temporal rise with photobleaching of the absorption spectrum of CV. We found convincing evidence that the absorption spectrum is inhomogeneous from the early part of the transient photobleaching.

Key Observation to Settling the Dispute. We concluded that the 2-fold absorption spectrum is inhomogeneous from the following experimental observations. In Figure 3 we show transient differential absorption (ΔOD) spectra and again a steady-state absorption spectrum of CV in methanol. The steady-state absorption spectrum has a maximum at 590 nm and a shoulder at 550 nm. The steady-state absorption spectrum in other normal alcohols was similar to that in methanol. The time

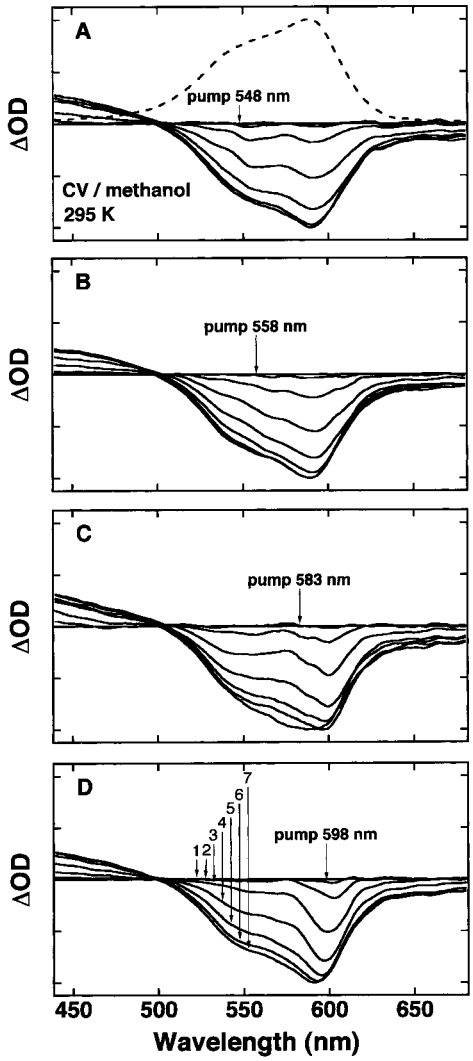

Figure 3. Transient differential absorption spectra (ΔOD) of CV in methanol at 295 K. The probe delay is from −600 (1) to 600 fs (7) at an interval of 200 fs as shown in the bottom recording. The bleaching maximums of (A), (B), (C), and (D) in optical density are −1.48, −1.52, −1.01, and −1.23, respectively.

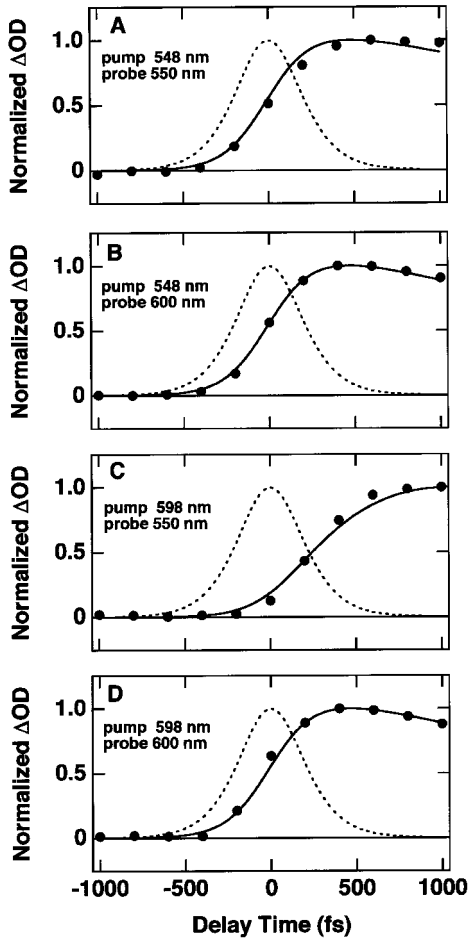

Figure 4. Time evolution of the spectral bleaching of CV in methanol at 295 K. The solid circles are the experimental data. The dotted lines represent the response function, the shape of which is assumed to be the shape of a sech^2 function. The full width of the half-maximum of the response function was about 450 fs. The solid lines are theoretical fits. The bleaching recovery times were 1.7 ps, which agrees with the previously reported data,[5,43] and 6.5 ps. A flattened top feature in the time evolution profile near 1000 fs was observed. This feature was interpreted in terms of a relaxation mechanism with one intermediate state other than the lowest excited singlet state.[5,43]

range of transient ΔOD spectra in Figure 3 was from −600 to +600 fs, corresponding to the temporal rise seen with bleaching.

The transient ΔOD spectra can roughly be divided into three regions: (i) in the wavelength region shorter than the absorption maximum and shoulder (≤500 nm), where transient absorption was dominantly observed; (ii) within the absorption band (500−620 nm), where bleaching was mainly observed; (iii) in the wavelength region longer than the absorption maximum and shoulder (≥620 nm), where stimulated emission gain was dominant. The shape of the bleaching spectrum at 600 fs was almost identical to the steady-state absorption spectrum, so that the stimulated emission gain and transient absorption would overlap less on the bleaching spectrum. For all of the pump wavelengths, a spectral hole at 600 nm and a spectral hole at 550 nm were observed, each of which corresponds to the absorption maximum and the shoulder, respectively. The pump light at 548 nm and that at 598 nm resonate with the shoulder at 550 nm and the peak at 600 nm, respectively. Note that the holes did not shift when pumped at 558 or 583 nm, both of which are out of resonance with the two holes.

Although the location of the holes was independent of the pumping wavelengths, the temporal rise of the holes was dependent on the pumping wavelengths. When pumped at 548 or 558 nm, the two holes appeared simultaneously (Figure 3A and B). When pumped at 598 nm, however, the hole at 550 nm appeared slower than that at 600 nm (Figure 3D). In addition, the hole at 600 nm shifted toward a shorter wavelength with time. We show the time evolution of the bleaching probed at 550 nm and that at 600 nm when pumped at 548 or 598 nm in Figure 4. Specifically, when pumped at 598 nm, the bleaching at 550 nm appeared with a time delay. In Figure 4C, we introduced a delay time for the rise of the bleaching τ_d into the fitting function as $1 - \exp(-t/\tau_d)$. The computed delay time was 500 fs. The origin of the time delay will be discussed in the section Summary of the Experimental Observations. Moreover, we measured delayed bleaching at 550 nm pumped at 598 nm in several normal alcohols to examine the viscosity dependence of the delay time (Figure 5). The delay time observed was practically constant (500 fs) irrespective of the alcohols used.

We have already concluded that the observed transient ΔOD spectrum is free from coherent artifacts and transient Raman gains.[16] Thus, we should consider the temporal rise of the spectral bleaching dependent on the pump and probe wavelengths as an intrinsic process in CV. If the ground state of CV is homogeneous, that is, the ground state is common for all

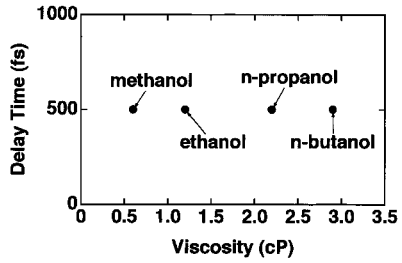

Figure 5. Rise delay time of the bleaching at 550 nm when pumped at 598 nm as a function of solvent viscosity at 295 K. The viscosity data were reported in ref 6.

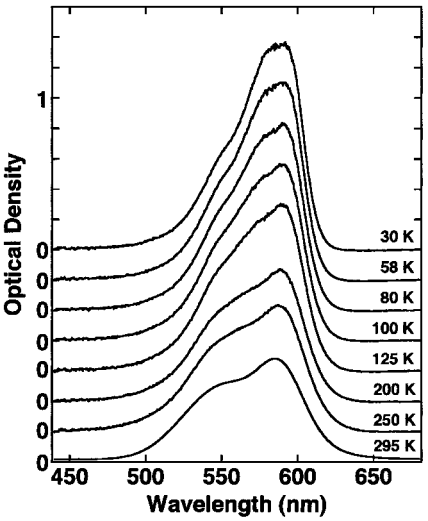

Figure 6. Temperature dependence of the absorption spectrum of CV in ethanol. The enhancement of the total OD with decreasing temperature may be due to the change of the refractive index of ethanol.

electronic transition, a decrease in the population in the ground state results in a decrease in all electronic transition intensities. Consequently, the bleaching should rise simultaneously irrespective of the pump and probe wavelengths. As a control experiment we observed transient spectral hole-burning for Nile blue and cresyl violet, both of which are more rigid molecules than CV. There was no pump-wavelength dependence temporal delay in the transient ΔOD spectra. Thus, our observations in Figures 3 and 4 strongly indicate the inhomogeneity of the ground state of CV in alcohols.

Decomposition of the 2-fold Inhomogeneous Absorption Spectrum into Each Homogeneous Component. Figure 6 shows the absorption spectra of CV in ethanol at several temperatures. With decreasing temperature the shoulder at 550 nm was reduced, whereas the peak at 590 nm was enhanced at all temperatures. This observation agreed with the previous findings.[48] Note that the shoulder did not disappear completely even at 30 K.

To get an insight into the observed bleaching dynamics, it is necessary to divide the inhomogeneous absorption spectrum into homogeneous components. The procedure to resolve the spectrum is as follows. The exchange of the intensity ratio between the shoulder and the peak in the absorption spectrum with decreasing temperature is assumed to be due to the modification of the thermal equilibrium between two ground-state populations. We also assume that almost all of CV are in the lower ground state at 30 K. On the other hand, the lowest singlet excited state (S_1) would be 2-fold degenerated according to the molecular orbital calculations of electronic states.[32,33,36] Furthermore, previous studies suggested that interaction of a polar

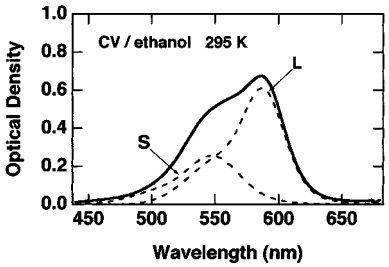

Figure 7. Gaussian deconvolution of the absorption spectrum of CV in ethanol at 295 K. The solid line represents the experimental data. The broken lines are the calculated spectra, each of which is composed of two Gaussian functions. The dotted line is the sum of the calculated spectra.

solvent molecule or a counteranion with a CV breaks the symmetry of the CV, thus lifting the degeneracy of the S_1 state.[34−36] Hence, the absorption spectrum of CV at 30 K would be composed of two electronic transitions from one ground state to two split S_1 states. For this reason, we fit two Gaussian curves on the absorption spectrum at 30 K. On the other hand, two isomers, each of which has an S_1 state split into two electronic states, should coexist at room temperature. Thus, the absorption spectrum at room temperature should be composed of four Gaussians.[51]

Figure 7 shows the result of the curve fitting for the absorption spectrum of CV in methanol at room temperature. The longer wavelength component denoted by "L" was well represented with two Gaussian curves whose maxima were 589 and 561 nm, respectively. The shorter wavelength component denoted by "S" was also composed of two Gaussian curves whose maxima are 550 and 524 nm, respectively. These two components L and S considerably overlap around 550 nm. The energy difference between the two ground states was estimated to be $\sim$200 cm^{-1} from the Arrhenius plot of the absorption intensity ratio between the two components. This value agrees well with that reported by Lewis and co-workers.[48] According to the energy difference, the population ratio between the two ground states is 9.7×10^{-3} from the Boltzmann factor at 30 K. This shows the adequacy of the assumption that there is little population in the higher energy ground state at 30 K.

Summary of the Experimental Observations. The observed bleaching dynamics should be explained with a model that has two ground-state isomers, each of which has two excited states. In Figure 8, we illustrate population dynamics when pumped at 548 or 598 nm. The pump light of 548 nm excites both ground states because the two absorption components overlap around 550 nm. Consequently, the bleaching should be caused all over the absorption spectrum. Similarly, the pump light of 558 nm also excites both isomers. On the other hand, when pumped at 598 nm, only the lower-energy isomer would selectively be excited. Thus, only the longer wavelength component L would bleach and therefore the populations of the two ground-state isomers would depart from thermal equilibrium. Note that the bleaching spectrum at 0 fs (marked with 4) in Figure 3D closely resembles the L component in Figure 7. If the potential barrier from the higher-energy ground state to the lower-energy ground state is comparable to kT at room temperature, the population of the higher-energy isomers can transfer to the lower ground state within a few picoseconds, assuming 10^{12} to 10^{13} s^{-1} as the preexponential factor of the rate process. Thus, the ground states of CV would quickly be in thermal equilibrium. The decrease in the population of the higher-energy ground state after the population transfer causes bleaching of the S component. The delay time (500 fs) of the rise of the bleaching at 550

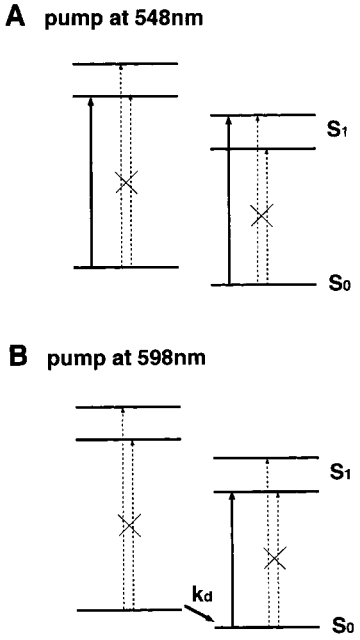

Figure 8. Energy level scheme of CV in alcoholic solutions. The arrows with solid lines represent electronic transitions by pump light or the population transfer from the higher ground state to the lower ground state. The arrows with broken lines are electronic transitions by probe light. The indicator "×" means the saturation of the transition; k_d is the isomerization rate, which is calculated at 1/500 $(fs)^{-1}$ by the curve fitting in Figure 4.

TABLE 1: Calculated Equilibrium Point of a Methanol Molecule on CV and Structure of CV

location of methanol	distance (Å)[a]	symmetry	total energy (eV)[b]
	∞	D_3 (planar)	−4377.72
central carbon	3.712	D_3 (planar)	−4377.81
nitrogen	4.101	D_3 (planar)	−4377.81

[a] The distance from the oxygen of methanol to CV. [b] Total energy of CV and a methanol molecule.

nm when pumped at 598 nm is ascribable to the population transfer time on the basis of the above model.

Theoretical Consideration of the Molecular Structure of CV in Alcohols. We examined the solvent effect on the symmetry of CV using a molecular orbital (MO) calculation. For simplicity only one methanol molecule was involved in the calculation. The results obtained are summarized in Tables 1−3. From the calculations, a free CV exhibits the D_3-symmetry propeller structure. When a methanol molecule is close to a CV, there are two stable methanol locations. One is 3.712 Å above the central carbon, and the other is 4.101 Å above one of the nitrogens. The structure of the CV in both cases remains that of D_3 symmetry (Table 1). The average distance between methanol molecules in the liquid phase was estimated to be 4.0656 Å from the specific gravity, assuming the uniform distribution of methanol molecules in the solution. One of the calculated data (4.101 Å) is almost the same as this value (4.0656 Å). However, when a cation is dissolved in a polar solvent, the solvent molecules would highly solvate the cation. It is therefore reasonable to expect that the distance between the CV cation and solvent molecules is shorter than the average methanol-to-methanol distance in pure methanol, which is almost the same as the calculated CV-to-methanol equilibrium distance. Moreover, MNDO calculations tend to underestimate the interaction between molecules,[19] so that the calculated value of the methanol equilibrium distance would be longer than the real value. Thus, we calculated the total energy and the structure of CV when a methanol molecule was closer to CV than the calculated equilibrium distance. When a methanol molecule is located at 2.0 Å above the central carbon, the structure is stable when the central carbon is 0.157 Å above the original sp^2 plane. On this occasion the CV takes the C_3 pyramidal structure. On the other hand, even if a methanol molecule is located 2.0 Å above one of the nitrogens, the structure of the CV remains that of D_3 symmetry (Table 2). When CV has D_3 symmetry, calculated absorption bands are 546.2 and 534.5 nm from lowest energy. When CV is deformed into C_3 symmetry, we obtained red-shifted bands 562.0 and 550.1 nm (Table 3). In the calculations of the absorption bands, no effects of a methanol other than the point-charge perturbation were taken into account.

TABLE 2: Calculated Structures of CV When a Methanol Distance Is Fixed at 2.0 Å

location of methanol	distance (Å)[a]	symmetry
central carbon	2.0 (fixed)	C_3 (pyramidal)
nitrogen	2.0 (fixed)	D_3 (planar)

[a] The distance from the oxygen of methanol to CV.

TABLE 3: Calculated Absorption Bands and Oscillator Strength of CV[a]

symmetry	λ_1 (nm)/f	λ_2 (nm)/f
D_3 (planar)	546.2/0.88	534.5/0.70
C_3 (pyramidal)	562.0/0.77	550.1/0.71

[a] λ_1, λ_2: absorption band. f: oscillator strength.

Construction of a Model for Ground-State Isomers. The D_3-symmetry propeller structure was experimentally identified as a ground-state structure of CV.[28−31] As another structure, the C_2-symmetry distorted propeller type was proposed.[48] Although this structure is easily expected from the molecular structure of CV, there was no evidence for the C_2 structure. Several studies[29−31,34−36] denied distinctly this structure. Here we propose another ground-state structure of CV based on the experimental observations, and the MO calculations of our own, together with the previous studies.

The origin of the ultrafast nonradiative relaxation of TPM dyes in the excited state is believed to be due to the torsional motion of the phenyl rings.[52] The bleaching recovery rate of CV depends sensitively on the solvent viscosity.[4−7] If the structural difference between the two isomers is due to the rotation or the torsion of the phenyl rings, the population transfer between the two isomers, or the change of structure, and the nonradiative relaxation rate of the excited state should become slower with increasing solvent viscosity. However, the rise time of the bleaching at 550 nm when pumped at 598 nm is practically constant even when the solvent was changed from methanol to *n*-butanol. The viscosity of butanol is about 5 times larger than that of methanol. The bleaching recovery time in butanol is about 4 times longer than that in methanol.[6] The insensitivity of the rise time to the solvent viscosity shows that the structural change between the two isomers is independent of, or at least not so sensitive to solvent viscosity. In other words, no large structural change like the torsion of the phenyl rings is needed to account for the difference between the two isomers of CV.

In general, a large amplitude vibrational mode with low frequency ($\leq$1000 cm^{-1}) would be concerned with the isomerization of ground states.[53] Moreover, the isomer of CV should have a structure especially affecting the shape of the absorption spectrum in the visible region. According to an expectation from the molecular structure of CV, the bending mode of the bonds

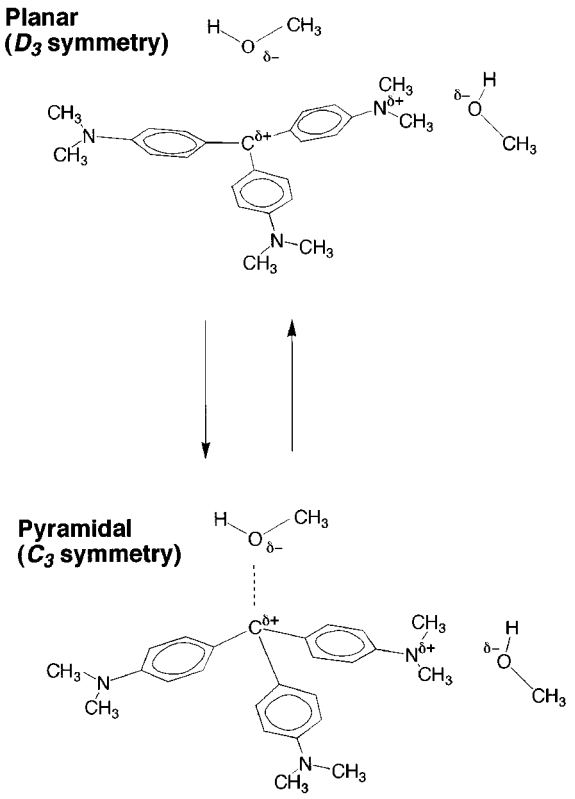

Figure 9. Proposed model of the ground-state structures of CV in alcohols discriminated by solvation equilibrium between an alcohol molecule and a CV cation.

from the central carbon to the three phenyl rings is a possible large amplitude vibration, except for the torsional motion of phenyl rings. The structural change accompanied by this vibration would be less affected by solvent viscosity than the torsional motion of the phenyl rings. Thus, we propose another ground-state structure of CV whereby the three bonds on the central carbon are bent with D_3-symmetry structure. Such a pyramidal structure has C_3 symmetry. Matsuoka and Yamaoka pointed out the possibility that CV takes a pyramidal structure, although they were not able to experimentally identify any ground-state isomers.[54]

We discuss how CV can assume the pyramidal structure. Because only D_3 symmetry was confirmed by the X-ray diffraction study of crystal samples,[28] the effects of alcohols should be taken into account as the cause of the inhomogeneity of the ground state of CV in solution. It is well-known that liquid alcohol forms a network (monomers, dimers, and higher structures) by hydrogen bonding.[55] A CV molecule solvated with alcohol is surrounded by a network of alcohol molecules. The CV molecule could have two or more solvation forms interacting with alcohol molecules. We suppose for simplicity that only a monomer alcohol solvates with the CV cation. We appreciate that the solvation model involving a single solvent molecule is an oversimplified picture. For all the simplicity, this model probably points out a fundamental picture of the solvation of CV molecules by methanol. The mechanism of solvation was previously discussed by Korppi-Tommola and co-workers.[34] A monomer−dimer equilibrium of alcohols modifies the solvation equilibrium between monomer alcohol and a CV cation. We therefore propose a model of the ground state of CV in Figure 9. When an alcohol molecule is solvated with a CV near the central carbon, the central carbon would be pulled toward the alcohol molecule. Thus, the CV may become a pyramidal structure. When the solvation between the central carbon and the alcohol molecule breaks, the CV has the propeller structure. Because the CV solvated with an alcohol should have rather lower energy, the pyramidal structure corresponds to the isomer of lower energy and the propeller structure corresponds to the isomer of higher energy. In both structures, other alcohol molecules should locate near one of the amino groups. The effect of a symmetry-breaking perturbation due to an interaction with alcohol molecules would cause the splitting of the degenerated S_1 state.[36] As a result, the absorption spectrum of each ground state would be composed of two absorption bands. Recently, Itaya and co-workers observed highly ordered arrays of CV molecules on iodine-modified Au(111) surfaces in solution by STM and found a bright spot at the position of the central carbon atom of CV.[56] On the basis of this observation a model may be possible that the bright spot is the counteranion (chloride), although the authors did not conclude the assignment of the bright spot. This model is equivalent to our solvation model that preferred solvation of a negative charge of methanol on the central carbon atom of CV is important for the C_3-symmetry pyramidal structure.

The results of our MO calculations showed that when a methanol molecule is located at 2.0 Å above the central carbon, CV has the C_3-symmetry pyramidal structure. Moreover, the calculated absorption bands for both D_3 and C_3 symmetry almost agree with the absorption bands for the S component and L component in Figure 7, respectively. Although many solvent molecules really surround a CV, this result strongly supports the possibility of CV having the pyramidal structure in alcohols.

The reason the C_3-symmetry structure has not been confirmed by the previous resonance Raman studies for CV in alcohol is probably as follows. The wavelengths of the Ar^+ laser used for excitation in the resonance Raman studies[30,31,36] were at the shorter edge of the absorption band, so that the excitation lights resonate only with the D_3-symmetry isomer. In the X-ray diffraction studies[28] the sample was not solution but crystal, so that the C_3-symmetry isomer could not be confirmed. The MO calculations[36] only denied the C_2-symmetry distorted propeller isomer and show lifting the degeneracy of the S_1 state. The results rather support our model that involves the split S_1 state. The time-resolved bleaching studies, which only concern the bleaching recovery dynamics, were not able to confirm the presence of isomers. The bleaching recovery times we observed, however, agree with the previous data.[6,43,44]

Concluding our findings, we propose the solvation isomers whereby CV in alcohols has D_3 or C_3 symmetries in the ground state. Furthermore, our model successfully explains almost all of the previously reported conflicting findings on the issue of the ground state isomers. Solvation will occur particularly for polar solute molecules in polar solvents. However, explicit observation of the solvation isomers will depend on the kinds of the solute molecules involved. Explicit appearance of the solvation isomers in CV would reflect the extremely flexible nature of TPM dyes even in the ground state. In general, organic molecules such as dye molecules are more flexible in the excited states than in the ground state because an electron in the bonding molecular orbital is promoted to a nonbonding molecular orbital. Thus, we expect fluorescence properties of TPM dyes to be exquisite probes for the immediate environments around them in condensed phase.

Probing Glass Transition in Alcohols and Polymers Using a TPM Dye

What Is Probed Using a TPM Dye? In recent years the importance of a supercooled state in liquids, which occurs well

TABLE 4: Melting Point (T_m), Critical Temperature (T_c), and Calorimetric Glass Transition Temperature (T_g) of the Alcohols and Polymers Selected

	T_m (°C)	T_c (°C)	T_g (°C)
1-propanol	−127	−143	−173
propylene glycol	−59	−68	−101
glycerol	17.8	−33	−80
poly(butadiene)		−65	−95
poly(vinyl acetate)			30
poly(methyl acrylate)			63
poly(methyl methacrylate)			114

above T_g has widely been recognized in condensed-matter physical chemistry.[57] One of the major theoretical considerations is provided by MCT.[58,59] Following the prediction of MCT a dynamical glass transition from ergodicity to nonergodicity should occur at T_c, which is several tens degrees above T_g. Stimulated by encouraging progress in the theoretical work, much effort has substantially been devoted to the experimental studies of the dynamics of glass-forming materials. The crossover phenomena at T_c were found by neutron scattering,[60] light scattering,[61] and viscosity measurements.[58,62] However, the crossovers observed are smooth in almost all of the macroscopic measurements. Thus, ambiguity remains in the precise positioning of T_c. To clearly identify the crossover point, it is favorable to use a molecular probe that is sensitive to the microscopic dynamics relevant to the dynamical transition.[10,11]

As briefly stated in the General Introduction, nonradiative relaxation of MG, from the S_1 state to the ground state, is strongly influenced by the solvent viscosity.[8−11] The fluorescence lifetime increases with increasing solvent viscosity from picoseconds to nanoseconds. At cryogenic temperatures (<77 K), the lifetime is only limited by the radiative transition, thus the fluorescence quantum yield being nearly unity. The viscosity-dependent nonradiative process is thought to be due to diffusive rotational motion of the phenyl rings in the S_1 state. Ben-Amotz and Harris,[5−7,63] and also Abedin and co-workers[8,9] concluded that the potential for the rotational motion of the phenyl rings is barrierless in the S_1 state. The barrierless potential makes the fluorescence lifetime of the dye molecule extremely sensitive to changes in solvent viscosity, because the friction from the surrounding solvent molecules is the only impediment to the rotational motion of the phenyl rings. Selected host matrixes for MG were several glass-forming materials such as 1-propanol (PR), propylene glycol (PG), and glycerol (GL) as monomers; polybutadiene (PB), poly(vinyl acetate) (PVAc), poly(methyl acrylate) (PMA), and poly(ethyl methacrylate) (PEMA) as polymers. The melting point (T_m) and the calorimetric glass transition temperature (T_g) are summarized for each compound in Table 4. The concentrations of MG doped in these glass-forming materials were $\sim 2 \times 10^{-5}$ M. The sample was first cooled to 10 K at a rate of 2 K/min, and then the fluorescence lifetime was measured from the lowest to the highest temperature step by step. We selected the spectral window for the lifetime measurement from 674 to 692 nm, within which no wavelength dependence of the fluorescence lifetimes was found in our experiment.

Contrasting Temperature Dependence of Nonradiative Decays of MG Doped in the Two Classes of the Glass-Forming Materials. In the higher temperature region than T_g the fluorescence decay curves of every sample were not fitted to a single exponential function or a stretched exponential function, but well fitted to a biexponential function (Figure 10A). The fast decay component decreases with decreasing temperature, and practically disappears at ~30 K above T_g for the monomers, PR, PG, and GL, and for the polymer without side chains, PB. On the other hand, for the polymers with side chains, PVAc, PMA, and PEMA, the fast decay component survived even far below T_g. At the temperatures lower than T_g each of the fluorescence decay curves was well fitted to a single-exponential function (Figure 10B); the lifetime approached a limiting value close to the radiative decay time. The nonradiative decay rate τ_{snr}^{-1} of the slow component was obtained by subtracting the radiative decay rate from the slow fluorescence decay rate when total decays were analyzed with a biexponential function.

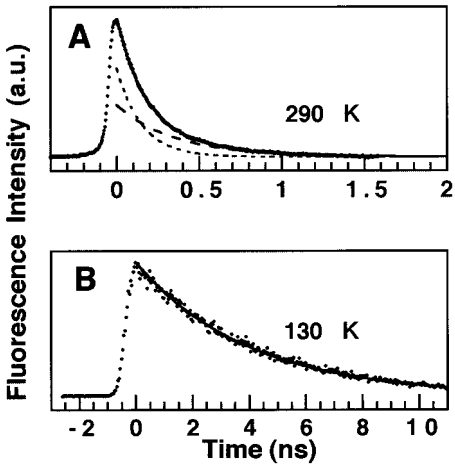

Figure 10. Fluorescence decay curves of MG doped in GL. Dotted lines are the experimental data, and solid lines are fitting curves. (A) In the higher-temperature region a biexponential decay curve is found, and the fast (short-dashed curve) and slow (long-dashed curve) components are also shown. (B) In the lower-temperature region the decay curve is well fitted to a single-exponential function.

Figure 11 shows the Arrhenius plots of the nonradiative decay time for the monomers, PR, PG, and GL, and for the polymer without side chains, PB. One recognizes without doubt three temperature regions in each curve. The lower crossover temperatures are close to each T_g, and the higher crossover temperatures are ~30−50 K above each T_g, which are reasonably attributed to T_c predicted by MCT. The reason the crossover at T_c was successfully identified using MG is attributed to the peculiar molecular structures of TPM dyes. The nonradiative relaxation time measured is limited by the time required for the diffusive rotation of phenyl rings to reach a sink in the S_1-state potential, from which deactivation occurs to the ground state. Because the S_1-state potential is barrierless and the required rotation for the nonradiative relaxation is very small (~10°), relaxation dynamics of the mediums was probed in the range of 10^{-11} to 10^{-8} s and the range of a few to several angstroms. Both of the ranges are just relevant to temporal and spatial windows for observing the dynamical glass transition predicted by MCT. This feature is quite different from other molecular probes. The temperature dependence of τ_{snr} was fitted to different equations in each temperature region. Above T_c it was fitted to a power law equation according to MCT, in the middle region between T_c and T_g it was fitted to the Vogel−Tamman−Fulcher (VTF) equation, and below T_g it was fitted to the Arrhenius equation. The Arrhenius dependence below T_g is consistent with other studies[8,9] of the molecular mobility in solid polymers.

For the other polymers, PVAc, PMA, and PEMA, which contain side chains, we could not identify any singularities above T_g. Figure 12 shows the Arrhenius plots of the nonradiative decay time of the slow components. For each of the three samples the nonradiative decay time at T_g is relatively short

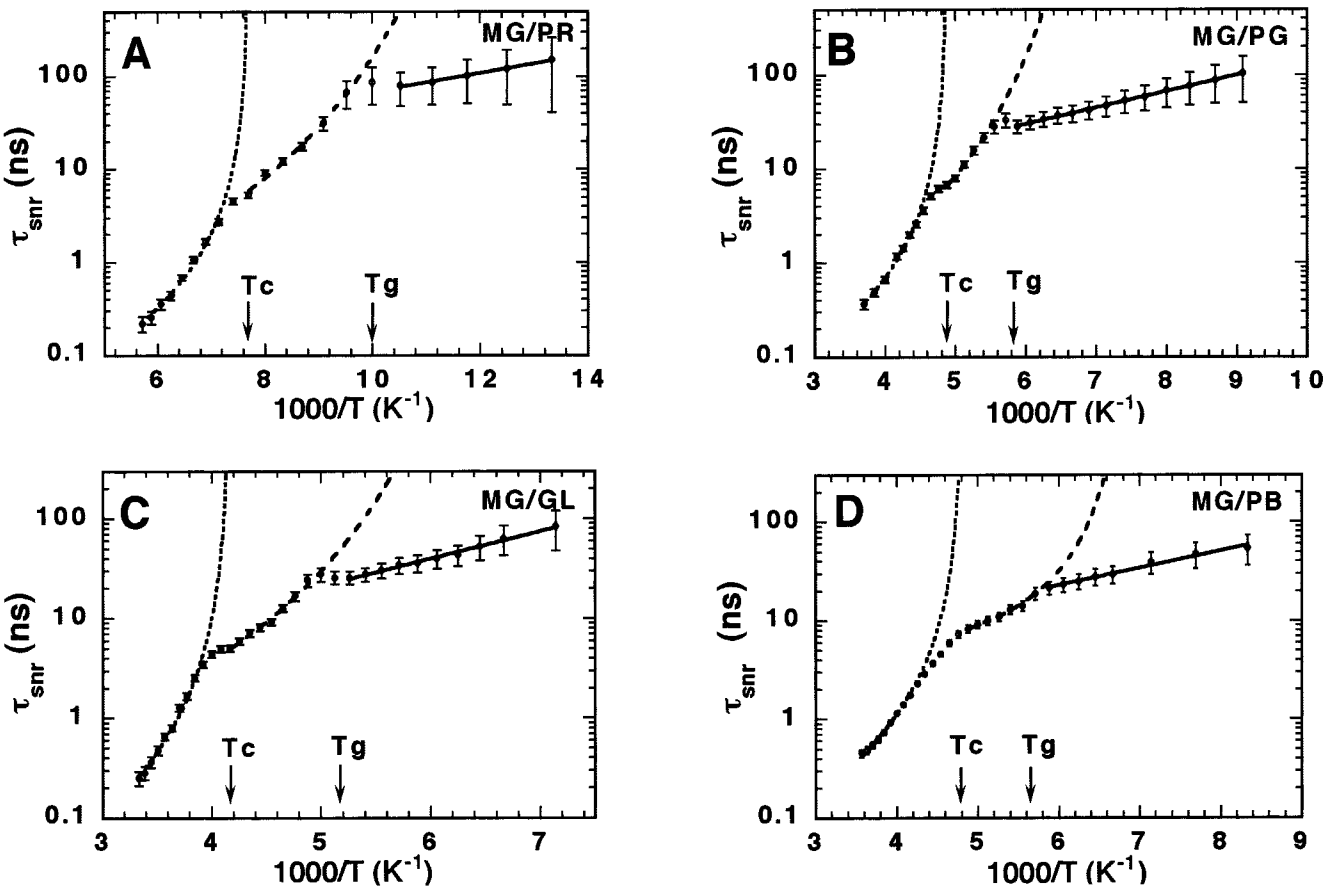

Figure 11. Arrhenius plots of the nonradiative decay time of the slow component of MG in (A) PR, (B) PG, (C) GL, and (D) PB as functions of temperature. The dotted, dashed, and solid curves represent the fittings of the power law, VTF equation, and Arrhenius law in the different temperature regions, respectively.

compared with those for the monomers and PB. This may be due to the fact that even below T_g the side-chain motions are not frozen yet, so that the microscopic viscosity experienced by MG molecules is not as large as that of the monomers and PB at their T_g's. We missed finding the crossover at T_c; however, the side-chain motions may mask it even if it exists. Moreover, the Arrhenius plot of the nonradiative decay time was not a straight line below T_g but showed two regions separated by a kink at a temperature several tens of degrees below T_g, which can be attributed to the freezing of the motion of side-chain groups.

Bimodality in the Dynamic Response of the Glass-Forming Materials. On the basis of the above observations we classified the glass-forming materials used into two groups: one group includes the monomers and the polymer without side chains; the other group includes the polymers with side chains. The Arrhenius plots of τ_{snr} in Figures 11and 12 show clearly the difference between the two groups. The difference comes from the fact that in the former group there is only translational or main-chain motions of the solvent molecules, whereas in the latter group there are side-chain motions in addition to the main-chain motions. In summary, by using MG molecules, we found the crossover at T_c predicted by MCT 30−50 K above T_g for the glass-forming monomers and the polymer without side chains. On the other hand, for the polymers with side chains, although we missed any singularities above T_g, we observed another kink below T_g, which is ascribable to the side-chain motion. The origin of the biexponential fluorescence decays is not fully understood yet, but may be attributed to the existence of the two sites in the alcohols and in the polymers with side chains. To conclude whether the biexponential fluorescence decay curve was due to averaging a heterogeneous distribution of single-exponential decay curves of each molecule or a homogeneous distribution of intrinsic biexponential decay curves of each molecule, we implemented imaging and time-resolved fluorescence measurement of individual CV molecules on a PMMA film.

Single Molecules Probing Bimodal Domain Structures in a Polymer Film

What Is Revealed Using Single-Molecule Probes? Ultrafast spectroscopy has been rapidly developed toward the femtosecond regime. An example of the development is described in the section Solvation Isomers of a TPM Dye in Alcohols, while ultrasensitive measurement has recently reached the single-molecule level.[12−15,25−27,64−77] The properties of individual molecules hidden under the ensemble of a large number of molecules, such as spectral diffusion and intensity fluctuations, were revealed by means of near-field[25,26,72,73] and far-field microscopies.[14,74−77] However, in these studies all of the selected chromophores were restricted to dye molecules or aromatic hydrocarbon molecules with a rigid molecular structure with high fluorescence efficiencies close to unity. The use of flexible dye molecules is useful for investigating microscopic dynamics of host matrixes as demonstrated in the section Probing Glass Transition in Alcohols and Polymers with a TPM Dye, because flexible dye molecules are more sensitive to the immediate surroundings than rigid molecules. In our single-molecule study we selected again CV molecules simply because the wavelength of the excitation light (532 nm) used is near the absorption maximum of CV.

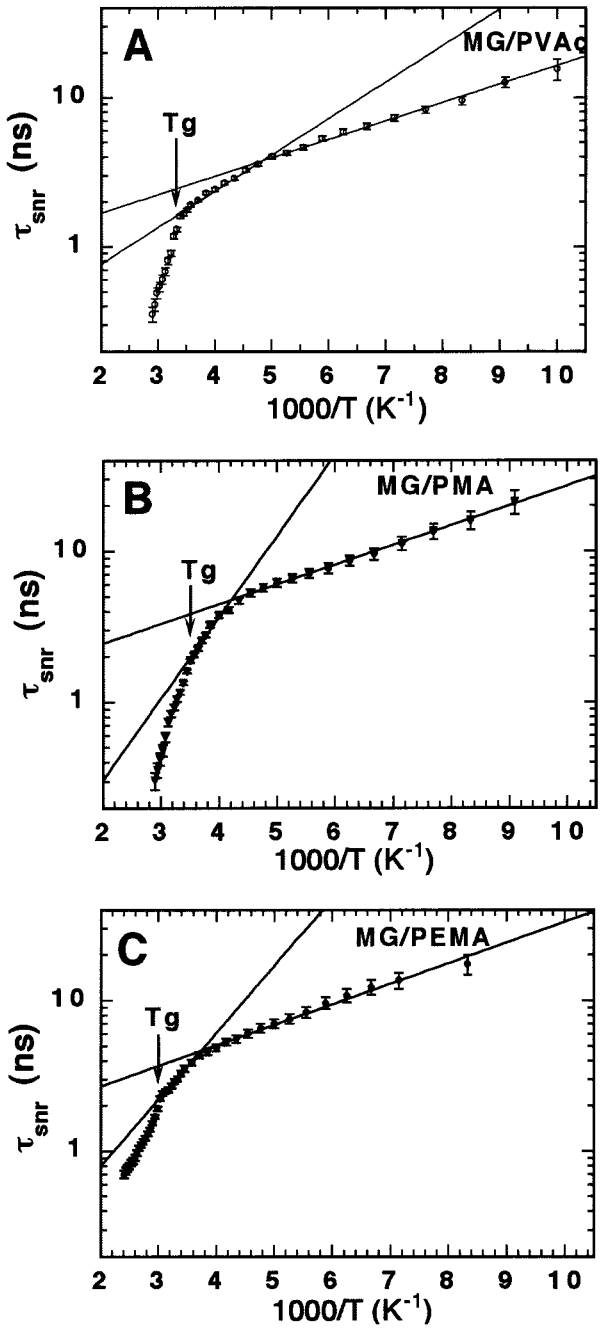

Figure 12. Arrhenius plots of the nonradiative decay time of the slow component of MG in (A) PVAc, (B) PMA, and (C) PEMA as functions of temperature. Below T_g the plots were found to have two regions of Arrhenius temperature dependence.

In our ensemble-averaged measurements, which were described in the previous section, the biexponential fluorescence decay curve was tentatively attributed to the heterogeneous structures of the host matrixes.[10,11] From the single-molecule measurements we concluded that the biexponential decay curve observed in the ensemble-averaged measurements comes from heterogeneous distribution of single exponential decay curves of individual CV molecules. Furthermore, we experimentally found for the first time the heterogeneous distribution, which is due to interaction of CV molecules with a PMMA film, shows a bimodal distribution. Recently, a theoretical study appeared, foreseeing bimodality of a supercooled liquid.[78]

Single Molecules Revealing Ensemble-Averaged Heterogeneity. Figure 13 shows a fluorescence decay curve of the ensemble of CV on a PMMA film. The curve was not fitted to a single-exponential function but was well fitted to a biexponential function, $I(t) = A_f \exp(-t/\tau_f) + A_s \exp(-t/\tau_s)$, where τ_f and τ_s are time constants and A_f and A_s are preexponential factors. We obtained $\tau_s = 1.76$ ns and $\tau_f = 0.43$ ns, and the ratio $A_s/A_f = 1.14$. Compared with the ultrafast decay times, which are within several picoseconds, of the excited state of CV in low-viscosity solvents such as methanol and ethanol,[4−7,37−47] the fluorescence lifetime of CV on a PMMA film increased more than 2 orders of magnitude,[8−11] and therefore, so did the fluorescence quantum efficiency. Enhancement of the fluorescence efficiency of CV on a PMMA film made it possible to observe single CV molecules. The number of fluorescent spots in an image linearly increased with the increasing concentration of methanol solution of CV that was spin-coated on PMMA films. This observation is evidence that fluorescence emission comes from individual CV molecules. Figure 14A shows fluorescent spots on a PMMA film that was spin-coated using a drop of 1 nM CV and Figure 14B is the three-dimensional plot of Figure 15A.

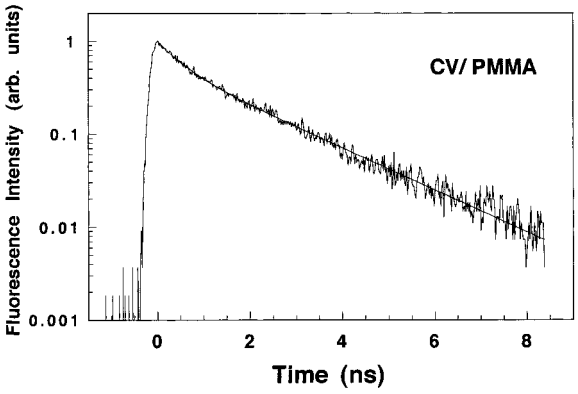

Figure 13. Fluorescence decay curve of CV located on a PMMA film obtained in the bulk measurement. The curve is well fitted to a biexponential function.

We obtained a histogram of fluorescence photocounts of individual CV molecules. The histogram shows a distinct bimodal distribution, as shown in Figure 15A. To examine whether the bimodal distribution is ascribable to the flexible structure of CV, we carried out a control experiment using Texas Red (TR) under the same conditions as used in the CV experiment. Owing to introduction of the oxygen bridge between two phenyl rings and immobilization of amino groups, TR has a rigid molecular structure. Figure 16B shows the histogram of fluorescence photocounts for TR, exhibiting only one maximum. The sharp contrast between two histograms must depend on the flexibility (or rigidity) of the molecular structures. Owing to the flexible structure, CV is extremely sensitive to the local viscosity of a PMMA film. On the other hand, TR is a highly fluorescent dye molecule whose fluorescence efficiency is close to unity[79] and, therefore, less sensitive to the local viscosity. It is not surprising that the photocounts of the maximum of the histogram for TR is smaller than those of the second maximum of the histogram for CV. The long-pass filter used cut a large portion of the fluorescence of TR, while almost all of the fluorescence from CV passed the filter owing to a large Stokes shift of the CV fluorescence.

For further evidence for observation of individual molecules and the site-dependent decay nature of CV, we carried out time-resolved fluorescence measurements at a single-molecule level. Indeed, an observation of the single-exponential lifetime for a given spot is evidence for the single-molecule imaging experiments. In our recent single-molecule study using the same experimental setup as that used in this article, we described

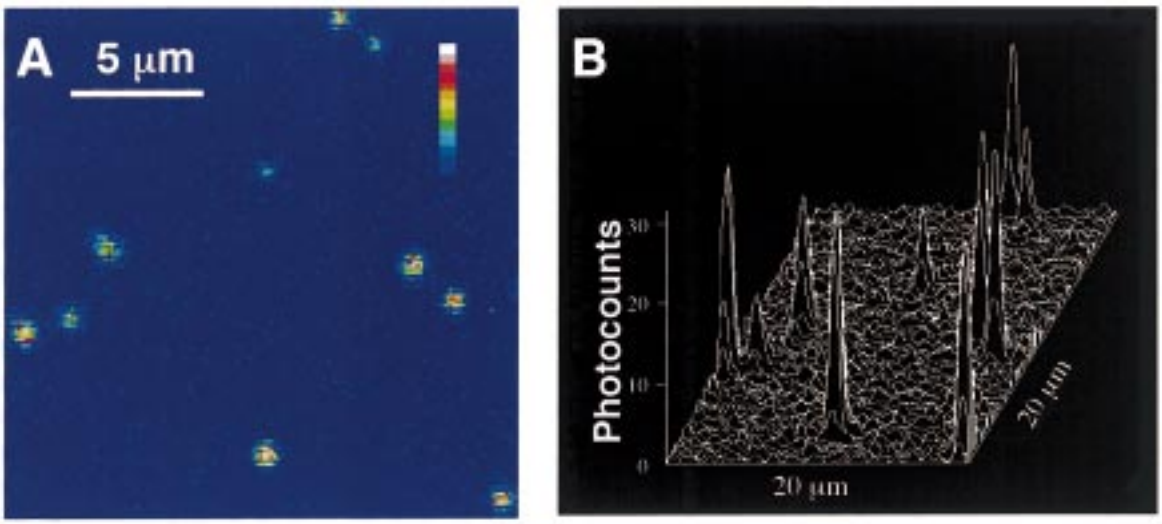

Figure 14. (A) Single-molecule fluorescence image of 1 nM CV spin coated on a PMMA film. The data accumulation time was 40 s. (B) Three-dimensional plot of the fluorescence image.

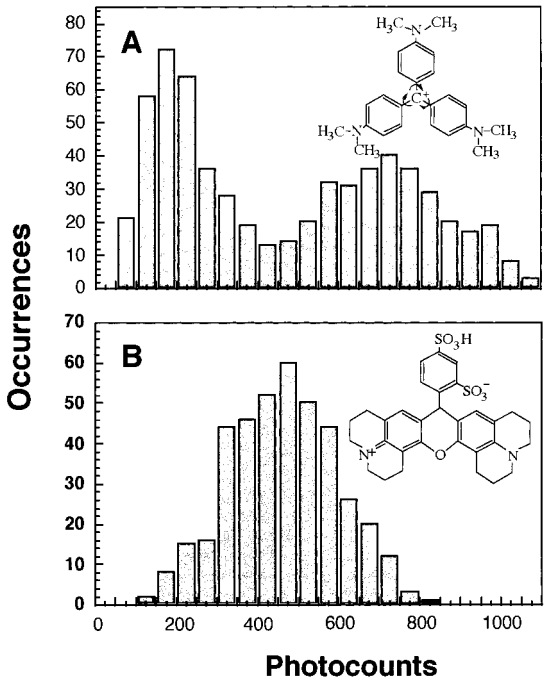

Figure 15. Fluorescence photocounts of individual molecules on a PMMA film versus the number of occurrences, (A) for CV and (B) for TR. The bin width is 50 counts. Molecular structures of CV and TR are shown in the insets of (A) and (B), respectively.

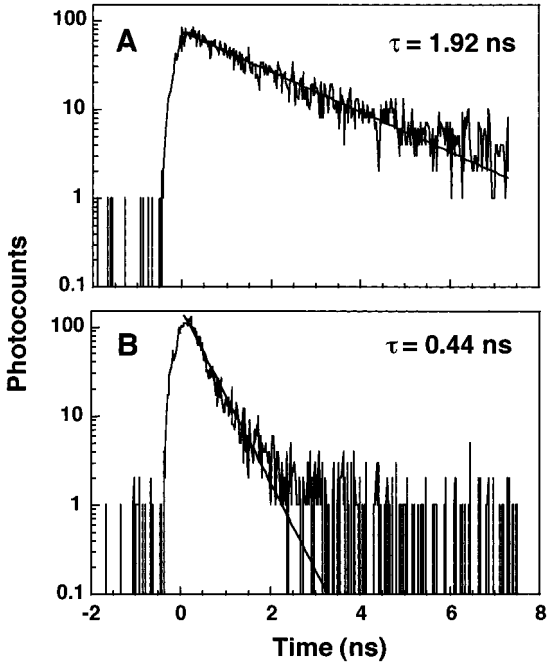

Figure 16. Selected fluorescence decay curves of single CV molecules on a PMMA film. The data accumulation time was 180 s. The curves are fitted to single-exponential functions: (A) corresponding to a strong fluorescent spot and (B) corresponding to a weak fluorescent spot.

estimation of fluorescence photocounts for a given spot incorporating collection efficiency and excitation parameters and staircase photobleaching of a given spot.[15] The observed fluorescence lifetimes varied from molecule to molecule: the fluorescence lifetime distributed in a wide range from 0.37 to 3.11 ns. Parts A and B of Figure 16 show representative fluorescence decay curves corresponding to a strong and a weak fluorescent spot, respectively. Each curve is well approximate to a single-exponential function, although a slight deviation from the single-exponential fitting can be seen, which might result from the intrinsic decay nature of CV itself.[4,10,62,80,81] The decay curves in Figure 16A,B are clearly different from each other and correspond to the fast and slow decay components obtained in the bulk measurement. For TR on a PMMA film, there is no such distinct difference in fluorescence decay curves such as CV. The fluorescence lifetime varies slightly from molecule to molecule within a range from 3.6 to 4.4 ns. This is understood by taking into account the fact that the fluorescence lifetime of TR is mainly determined by the radiative lifetime, whereas that of CV is affected by the internal conversion that is sensitive to the local environment.

The finding that the histogram of CV has a bimodal distribution means that, although the interaction of individual CV molecules with PMMA are different from site to site, the sites of a PMMA matrix are roughly separated into two classes, namely, viscous and less-viscous sites. The less-viscous sites may be attributed to the sites where the side chains of the polymers move to some extent freely, while the less-viscous sites may correspond to the sites where the side-chain motion is suppressed. The background for the above inference that the local viscosity of each site is associated with the degree of side chain motion was addressed in previous studies.[11,82] They

concluded that some side-chain motions still occur at temperatures lower than T_g and the heterogeneous nature of the degree of side-chain motion causes the biexponential fluorescence decays. Our single-molecule measurements were carried out at room temperature. Some side-chain motions causing bimodal local viscosity would be possible, although the room temperature (296 K) is much lower than $T_g = 387$ K of PMMA.[18]

Numerical Consistency between Single-Molecule and Bulk Measurements. If the two sites were roughly separated at the minimum of the histogram in Figure 15A, the ratio of the site numbers between high-viscosity and low-viscosity sites was estimated to be 0.98. This value is compatible with the amplitude ratio A_s/A_f (=1.14) obtained in the bulk measurement. The mean photocounts of CV located at nonviscous (P_N) and viscous (P_V) sites were calculated by averaging the photocounts corresponding to the higher- and lower-photocount maximums, respectively. We obtained the ratio $P_N/P_V = 3.73$, which is in agreement with the ratio between the fluorescence lifetimes $\tau_s/\tau_f = 4.09$ obtained in the bulk measurement within errors. Thus, the result of single-molecule imaging implies that the nonexponential fluorescence decay of CV in the bulk measurement is due to the ensemble averaged site-dependent single exponential decays of individual molecules.

Summary of the Single-Molecule Study. The experimental findings illustrated that the interaction between CV molecules and the polymer matrix shows strongly site-dependent and bimodal nature. As a result, the site-dependent nonradiative process of individual CV molecules is responsible for biexponential fluorescence decay curves of CV observed in the bulk measurement. Thus, our single-molecule study presented in this article would open up new possibilities in the experimental study of dynamic response of condensed matter such as polymers and liquid. We further expect that dye molecules with flexible molecular structures such as CV may be used as sensitive local probes for investigating microscopic dynamics of various host mediums.

Concluding Remarks

We presented three topics that were studied by means of modern experimental techniques, including ultrashort pulse lasers and single-photon sensitive detectors plus time-honored TPM dye molecules. The proposed solvation isomers should be added as a novel class of isomers in the family of isomerism. The use of TPM dye molecules as probes of nanoenvironment proved to be useful especially when they were prepared in dilution, that is, in the single-molecule condition. In general, possible advantages of dye molecules as probes are not only as beacons simply visualizing invisibles but also as reporters of chemical information such as pH and of physical information such as viscosity. On the other hand, possible disadvantages are being liable to photobleaching and intrinsic small Stokes shifts, causing reduced signal-to-noise ratios. Recent progress in the use of rare earth chelate compounds[83] and quantum dots[84,85] partly offsets the disadvantages of dye molecules because they are against photobleaching and showing large Stokes shifts. Although quantum dots and rare earth chelate compounds are useful as beacons, they would lack, at present, the function of reporters telling us chemical and physical information of the nanoenvironment. Thus, we expect in the future the advent of probes combining the advantages of dye molecules, quantum dots, and rare earth chelate compounds.

Acknowledgment. This work was performed under the management of ATP in JRCAT, and partly supported by the New Energy and Industrial Technology Development Organization (NEDO).

References and Notes

(1) Duxbury, D. F. *Chem. Rev.* **1993**, *93*, 381.
(2) Bush, G. E.; Rentzepis, P. M. *Science* **1976**, *194*, 276.
(3) Migus, A.; Antonetti, A.; Etchepare, J.; Hulin, D.; Orszag, A. *J. Opt. Soc. Am. B* **1985**, *2*, 584.
(4) Sundström, V.; Gillbro, T. *J. Chem. Phys.* **1984**, *81*, 3463.
(5) Ben-Amotz, D.; Harris, C. B. *Chem. Phys. Lett.* **1985**, *119*, 305.
(6) Ben-Amotz, D.; Harris, C. B. *J. Chem. Phys.* **1987**, *86*, 4856.
(7) Ben-Amotz, D.; Jeanloz, R.; Harris, C. B. *J. Chem. Phys.* **1987**, *86*, 6119.
(8) Abedin, K. M.; Ye, J. Y.; Inouye, H.; Hattori, T.; Nakatsuka, H. *J. Lumin.* **1995**, *64*, 135.
(9) Abedin, K. M.; Ye, J. Y.; Inouye, H.; Hattori, T.; Sumi, H.; Nakatsuka, H. *J. Chem. Phys.* **1995**, *103*, 6414.
(10) Ye, J. Y.; Hattori, T.; Inouye, H.; Ueta, H.; Nakatsuka, H.; Maruyama, Y.; Ishikawa, M. *Phys. Rev.* **1996**, *B 53*, 8349.
(11) Ye, J. Y.; Hattori, T.; Nakatsuka, H.; Maruyama, Y.; Ishikawa, M. *Phys. Rev.* **1997**, *B 56*, 5286.
(12) Ishikawa, M.; Hirano, K.; Hayakawa, T.; Hosoi, S.; Brenner, S. *Jpn. J. Appl. Phys.* **1994**, *33*, 1571.
(13) Ishikawa, M.; Watanabe, M.; Hayakawa, T.; Koishi, M. *Anal. Chem.* **1995**, *67*, 511.
(14) Ye, J. Y.; Ishikawa, M.; Yogi, O.; Okada, T.; Maruyama, Y. *Chem. Phys. Lett.* **1998**, *288*, 885.
(15) Ishikawa, M.; Yogi, O.; Ye, J. Y.; Yasuda, T.; Maruyama, Y. *Anal. Chem.* **1998**, *70*, 5198.
(16) Ishikawa, M.; Maruyama, Y. *Chem. Phys. Lett.* **1994**, *219*, 416.
(17) Maruyama, Y.; Ishikawa, M.; Satozono, H. *J. Am. Chem. Soc.* **1996**, *118*, 6257.
(18) When PMMA was formed in thin films (20−40 nm), T_g goes up by ~10 °C (Grohens, Y.; Brogly, M.; Labbe, C.; David, M.-O.; Schultz, J. *Langmuir* **1998**, *14*, 2929).
(19) Stewart, J. J. P. *J. Comput. Chem.* **1989**, *10*, 209 and 221.
(20) Bene, J. D.; Jaffe, H. H. *J. Chem. Phys.* **1968**, *48*, 807 and 4050
(21) Nishimoto, K. *Bull. Chem. Soc. Jpn.* **1993**, *66*, 1876.
(22) Foresman, J. B.; Frisch, A. *Exploring Chemistry with Electronic Structure Methods*, 2nd ed.; Gaussian: 1996; Chapter 6.
(23) Pariser, R.; Parr, R. G. *J. Chem. Phys.* **1953**, *21*, 466 and 767.
(24) Pople, J. A. *Trans. Faraday Soc.* **1953**, *49*, 1375.
(25) Betzig, E.; Chichester, R. J. *Science* **1993**, *262*, 1422.
(26) Trautman, J. K.; Macklin, J. J. *Chem. Phys.* **1996**, *205*, 221.
(27) Ha, T.; Enderle, Th.; Chemla, D. S.; Selvin, P. R.; Weiss, S. *Phys. Rev. Lett.* **1996**, *77*, 3979.
(28) Gomes de Mesquita, A. H.; MacGillavry, C. H.; Eriks, K. *Acta Crystallogr.* **1965**, *18*, 437.
(29) Dekkers, H. P. J. M.; Kielman-Van Luyt, E. C. M. *Mol. Phys.* **1976**, *31*, 1001.
(30) Angeloni, L.; Smulevich, G.; Marzocchi, M. P. *J. Raman Spectrosc.* **1979**, *8*, 305.
(31) Angeloni, L.; Smulevich, G.; Marzocchi, M. P. *J. Mol. Struct.* **1980**, *61*, 331.
(32) Looney, C. W.; Simpson, W. T. *J. Am. Chem. Soc.* **1954**, *76*, 6293.
(33) Adam, F. C.; Simpson, W. T. *J. Mol. Spectrosc.* **1959**, *3*, 363.
(34) Korppi-Tommola, J.; Yip, R. W. *Can. J. Chem.* **1981**, *59*, 191.
(35) Korppi-Tommola, J.; Kolehmainen, E.; Salo, E.; Yip, R. W. *Chem. Phys. Lett.* **1984**, *104*, 373.
(36) Lueck, H. B.; McHale, J. L.; Edwards, W. D. *J. Am. Chem. Soc.* **1992**, *114*, 2342.
(37) Magde, D.; Winsor, M. W. *Chem. Phys. Lett.* **1974**, *24*, 144.
(38) Yu, W.; Pellegrino, F.; Grant, M.; Alfano, R. R. *J. Chem. Phys.* **1977**, *67*, 1766.
(39) Grzybowski, J. M.; Sugamori, S. E.; Williams, D. F.; Yip, R. W. *Chem. Phys. Lett.* **1979**, *65*, 456.
(40) Cremers, D. A.; Windsor, M. W. *Chem. Phys. Lett.* **1980**, *71*, 27.
(41) Menzel, R.; Hoganson, C. W.; Windsor, M. W. *Chem. Phys. Lett.* **1985**, *120*, 29.
(42) Mokhtari, A.; Fini, L.; Chesnoy, J. *J. Chem. Phys.* **1987**, *87*, 3429.
(43) Martin, M. M.; Breheret, E.; Nesa, F.; Meyer, Y. H. *Chem. Phys.* **1989**, *130*, 279.
(44) Martin, M. M.; Plaza, P.; Meyer, Y. H. *Chem. Phys.* **1991**, *153*, 297.

(45) Martin, M. M.; Plaza, P.; Meyer, Y. H. *J. Phys. Chem.* **1991**, *95*, 9310.
(46) Vogel, M.; Rettig, W. *Ber. Bunsen-Ges. Phys. Chem.* **1985**, *89*, 962.
(47) Vogel, M.; Rettig, W. *Ber. Bunsen-Ges. Phys. Chem.* **1987**, *91*, 1241.
(48) Lewis, G. N.; Magel, T. T.; Lipkin, D. *J. Am. Chem. Soc.* **1942**, *64*, 1774.
(49) Clark, F. T.; Drickamer, H. G. *J. Chem. Phys.* **1984**, *81*, 1024.
(50) Clark, F. T.; Drickamer, H. G. *J. Phys. Chem.* **1986**, *90*, 589.
(51) Because our experiments on a change in the absorption spectrum involved a large number of molecules, we preferred Gaussians. The use of Lorentzians is probably suitable for curve fitting calculation reproducing overlapped spectra when the number of the molecules involved is sparse, such as in single-molecule high-resolution spectroscopy of impurity centers in host crystals at low temperatures (<10 K) (Moerner, W. E. *Acc. Chem. Res.* **1996**, *29*, 563−571).
(52) Förster, T.; Hoffmann, G. *Z. Phys. Chem. NF* **1971**, *75*, 63.
(53) Hollas, J. M. *Chem. Soc. Rev.* **1993**, 371.
(54) Matsuoka, Y.; Yamaoka, K. *Bull. Chem. Soc. Jpn.* **1979**, *52*, 2244.
(55) Pierce, W. C.; MacMillan, D. P. *J. Am. Chem. Soc.* **1938**, *60*, 779.
(56) Batina, N.; Kunitake, M.; Itaya, K. *J. Electroanal. Chem.* **1996**, *405*, 245.
(57) Ediger, M. D.; Angell, C. A.; Nagel, S. R. *J. Phys. Chem.* **1996**, *100*, 13200.
(58) Gotze, W.; Sjoren, L. *Rep. Prog. Phys.* **1992**, *55*, 241.
(59) Gotze, W. In *Liquids, Freezing and the Glass Transition*; Hansen, J. P., Levesque, D., Zinn-Justin, J., Eds.; North-Holland: Amsterdam, 1991; p 287.
(60) Richter, D.; Frick, B.; Farago, B. *Phys. Rev. Lett.* **1988**, *61*, 2465.
(61) Du, W. M.; Li, G.; Cummins, H. Z.; Fuchs, M.; Toulouse, J.; Knauss, L. A. *Phys. Rev.* **1994**, *E49*, 2192.
(62) Taborek, P.; Kleiman, R. N.; Bishop, D. J. *Phys. Rev.* **1986**, *B34*, 1835.
(63) Ben-Amotz, D.; Harris, C. B. *J. Chem. Phys.* **1987**, *86*, 5433.
(64) Shera, E. B.; Seitinger, N. K.; Davis, L. M.; Keller, R. A.; Soper, S. A. *Chem. Phys. Lett.* **1990**, *175*, 553.
(65) Basché, T.; Moerner, W. E.; Orrit, M.; Talon, T. *Phys. Rev. Lett.* **1992**, *69*, 1516.
(66) Orrit, M.; Bernard, M.; Personov, R. I. *J. Phys. Chem.* **1993**, *97*, 10256.
(67) Güttler, F.; Imgartinger, T.; Plakhotnik, T.; Renn, A.; Wild, U. P. *Chem. Phys. Lett.* **1994**, *217*, 393.
(68) Nie, S.; Chiu, D. T.; Zare, R. N. *Science* **1994**, *266*, 1018.
(69) Xu, X. H.; Yeung, E. S. *Science* **1997**, *275*, 1106.
(70) Enderlein, J.; Goodwin, P. M.; Order, A. V.; Ambrose, W. P.; Erdmann, R.; Keller, R. A. *Chem. Phys. Lett.* **1997**, *270*, 464.
(71) Nie, S.; Emory, S. R. *Science* **1997**, *275*, 1102.
(72) Xie, X. S.; Dunn, R. C. *Science* **1994**, *265*, 361.
(73) Bian, R. X.; Dunn, R. C.; Xie, X. S.; Leung, P. T. *Phys. Rev. Lett.* **1995**, *75*, 4772.
(74) Macklin, J. J.; Trautman, J. K.; T. D. Harris, T. D.; L. E. Brus, L. E. *Science* **1996**, *272*, 255.
(75) Funatsu, T.; Harada, Y.; Tokunaga, M.; Saito, K.; Yanagida, T. *Nature* **1995**, *374*, 555.
(76) Lu, H. P.; Xie, X. S. *Nature* **1997**, *385*, 143.
(77) Dickson, R. M.; Cubitt, A. B.; Tsien, R. Y.; Moerner, W. E. *Nature* **1997**, *388*, 355.
(78) Bhattachayya, S.; Bagchi, B. *J. Chem. Phys.* **1997**, *106*, 7262.
(79) Soper, S. A.; Nutter, H. L.; Keller, R. A.; Davis, L. M.; Shera, E. B. *Photochem. Photobiol.* **1993**, *57*, 972.
(80) Kemnitz, K.; Yoshihara, K. *J. Phys. Chem.* **1990**, *94*, 8805.
(81) Bagchi, B.; Fleming, G. R.; Oxtoby, D. W. *J. Chem. Phys.* **1983**, *78*, 7375.
(82) Schmidt-Rohr, K.; Kulik, A. S.; Beckham, H. W.; Ohlemacher, A.; Pawelzik, U.; Boeffel, C.; Spiess, H. W. *Macromolecules* **1994**, *27*, 7, 4733.
(83) Yuan, J.; Matsumoto, K. *Anal. Chem.* **1998**, *70*, 596.
(84) Bruchez, M., Jr.; Moronne, M.; Gin, P.; Weiss, S.; Alivisatos, A. P. *Science* **1998**, *281*, 2013.
(85) Chan, W. C. W.; Nie, S. *Science* **1998**, *281*, 2016.